PCCP

PAPER

View Article Online
View Journal | View Issue

Cite this: *Phys. Chem. Chem. Phys.*, 2017, **19**, 24230

Monolayer BC_2: an ultrahigh capacity anode material for Li ion batteries†

Deya Das, ‡[a] Rahul P. Hardikar,‡[a] Sang Soo Han,[b] Kwang-Ryeol Lee[b] and Abhishek K. Singh *[a]

Received 3rd July 2017,
Accepted 14th August 2017

DOI: 10.1039/c7cp04451h

rsc.li/pccp

There is great interest in developing promising candidate materials for high-capacity, low cost, environmentally friendly, longer cycle life anodes for lithium ion batteries. Due to better Li adsorption properties than graphene, boron doped graphene has been considered to be an attractive anode material for Li-ion batteries. Using first principles density functional theory calculations, we investigate the effect of increasing boron concentration on the gravimetric capacity of monolayered boron doped carbon sheets. The calculations are performed for uniformly boron doped carbon sheets, BC_x (x = 7, 5, 3, 2 and 1) as well as their non-uniformly doped counterparts, which are found to be energetically preferable for x = 5, 2 and 1. Our results indicate pronounced enhancement in gravimetric capacity with increasing concentration of B, up to x = 2. The storage capacity of the uniformly doped BC_2 turns out to be the highest ever reported for B doped graphene sheets, which is 1.9 times (1667 mA h g^{-1}) that of the previously reported value for BC_3 (*J. Phys. Chem. Lett.*, 2013, **4**, 1737–1742). This dramatic increase in the capacity of uniformly doped BC_2 occurs because of the availability of significantly more empty states above the Fermi level compared to the other BC_x sheets. Moreover, the diffusion energy barriers and open circuit voltage are found to be lower in uniformly doped BC_2, leading to better Li kinetics. For x = 1, Li binds very strongly to the uniformly doped BC and higher diffusion energy barriers are found for non-uniformly doped BC, rendering them ineffective as anode materials. Our study reveals that BC_2 is the most promising candidate as an anode material for Li ion batteries owing to its high Li storage capacity combined with low diffusion barrier and low open circuit voltage.

1 Introduction

The current generation lithium (Li)-ion batteries utilize graphite as an anode material due to its low cost, high coulombic efficiency, and mechanical stability. However, the capacity of a graphite anode is very low (372 mA h g^{-1})[1,2] and it cannot meet the requirements of electric vehicles, power grids, *etc.*[3–7] Much effort has been devoted to unearthing new carbon based materials that can meet the required high capacity. One way to accomplish enhanced capacity is *via* nano-structuring of these materials, leading to an increase in the surface area, shorter diffusion paths and greater mobility.[3,8–12] Although multilayers ($\geq$4)[13,14] of graphene show high capacity ($\sim$540–1264 mA h g^{-1}), a single layer of graphene does not adsorb Li as shown in theoretical as well as *in situ* Raman spectra studies.[10,15,16] Defect mediated modification of graphene can drastically alter the properties and can make it suitable for Li adsorption. A significant amount of research has shown that intrinsic and/or extrinsic defects can induce Li adsorption in graphene *via* active sites.[10,11,17–19] Introduction of extrinsic defects *via* chemical doping is also an effective way of achieving enhanced Li adsorption.[16,20,21] Typically, dopants such as boron (B)[22–24] and nitrogen (N)[25,26] with a similar size to that of C atoms preserve the honeycomb arrangement of graphene[20,27] and have been reported to enhance the energy storage. Electronically, N doping in graphene leads to an excess of electrons (n-type), while B doping gives an electron deficient lattice (p-type).[20] However, N doping shows very high adsorption energy for Li, giving rise to poor kinetics of Li-ions.[10] On the other hand, boron doped graphene due to lack of electrons tends to adsorb Li readily within the optimal limits of binding energy.[24,28] Wu *et al.*[29] have experimentally reported that 0.88% B doping and 3.06% N doping in graphene leads to capacities of 1227 mA h g^{-1} and 872 mA h g^{-1} after 30 cycles.

Boron doped graphitic structures have been extensively studied in the literature for their hardness[30–34] and superconducting properties.[35,36] Recently, these structures have also been explored

[a] *Materials Research Centre, Indian Institute of Science, Bangalore 560012, India. E-mail: abhishek@mrc.iisc.ernet.in*
[b] *Korea Institute of Science and Technology, Hwarangno 14-gil 5, Seongbuk-gu, Seoul 136-791, Korea*

† Electronic supplementary information (ESI) available. See DOI: 10.1039/c7cp04451h

‡ These authors contributed equally to this work.

for electrochemical energy storage applications. Hence, greater emphasis has been placed on finding the structure of the B doped/alloyed carbon bulk and sheets. Using the swarm algorithm, Wang *et al.* proposed bulk structures for several different concentrations of B in boron doped carbon compounds.[37] Stable 2D allotropes of boron doped carbon (BC_x with $x \geq 1$) sheets have been reported theoretically which preserve the maximum number of hexagons.[38] Experimentally, however, only mono-layers of BC_3[39] and BC_5[40] have been synthesized so far, among which monolayer BC_3 has been studied extensively.[41–43] B doping in graphene has been reported to show enhanced performance as an anode material compared to pristine graphene.[29,44,45] Rodríguez *et al.* suggested that boron doping in graphite foams is beneficial for Li anodes.[46] In particular, B_4C[47] shows better reversibility due to enhanced conductivity and lowering of the Fermi level[48] although it shows low capacity (315 mA h g^{-1}) compared to graphite. Theoretically, by doping pristine graphene with B and N atoms as well as by introducing different B–B pairs and B–N pairs, the specific capacity has been reported to be enhanced significantly.[49] Another similar study on graphyne also shows that boron doping enhances Li storage and electrochemical performance.[50] Liu *et al.* demonstrated that a mono-layer of BC_3 shows about 2.5 times increase in the Li storage capacity compared to graphite.[16] Recently, borophene, a boron counterpart of graphene, has drawn much attention as a promising anode material.[51–55] Although, the diffusion barrier for Li is reported to be very low, 0.007 eV,[52] the high Li adsorption energy of −2.68 eV in *Pmmn* borophene sheets will hinder the de-lithiation process during discharging.

The aforementioned studies establish the beneficial effect of B doping on electrochemical performance of carbon based anode materials. Experimental and theoretical studies so far have been conducted only for a fixed amount of B doping. However, a systematic understanding of the effect of B concentration on the capacity of the carbon based nanostructure is still lacking. Here, we conduct an extensive study by considering uniformly doped as well as energetically preferable non-uniformly doped BC_x mono-layers, where x = 7, 5, 3, 2 and 1. Our results indicate that an increase in the concentration of B in BC_x significantly enhances the capacity of the carbon based anode materials up to x = 2. In uniformly doped BC, a higher concentration of B leads to a very strong adsorption of Li. On the other hand, although the Li adsorption energy is moderate in non-uniformly doped BC, the high diffusion barrier for Li makes it less effective for anode materials. We find that uniformly doped BC_2 shows the highest ever reported capacity of 1667 mA h g^{-1} for B doped graphene, much higher than the previously reported capacity[16] of BC_3. Partial density of states calculations reveal that uniformly doped BC_2 has more empty states above the Fermi level compared to all other sheets with different stoichiometry. Hence, more Li can easily donate electrons resulting in high Li storage capacity. The diffusion barriers are also lowered with an increase in B concentration for uniformly doped BC_x layers, being a minimum of ~0.41 eV for uniformly doped BC_2 and BC_3. Furthermore, uniformly doped BC_2 shows the lowest average open circuit voltage (OCV) of 0.43 V leading to extremely high energy density of 5541 W h kg^{-1}. Through our study, we not only find the optimal concentration which shows the best electrochemical performance but also developed a fundamental understanding about the role of boron doping on the Li storage capacity and kinetics in boron doped graphene. These results can be used as a benchmark for designing graphene based anode materials with varying concentrations of boron.

2 Methodology

The calculations have been performed using density functional theory (DFT) as implemented in the Vienna ab initio simulation package (VASP).[56,57] The electron–ion interactions and electronic exchange correlations are incorporated by using an all-electron projector augmented wave potential (PAW)[58] and the Perdew–Burke–Ernzerhof (PBE) generalized gradient approximation (GGA),[59,60] respectively. The periodic images were separated by 15 Å vacuum in the direction perpendicular to the plane of the sheet to avoid any spurious interactions among the images. Geometry optimizations were performed using the conjugate gradient (CG) scheme, until the forces on each atom are of the order of 10^{-3} eV $Å^{-1}$. The kinetic energy cutoff for the plane wave was set to 400 eV to ensure the accuracy of the calculations. The Brillouin zone has been sampled by a 5 × 5 × 1 *k*-grid using a Monkhorst–Pack scheme for uniformly doped BC_x sheets for relaxation calculations. For non-uniformly doped BC_x sheets, a *k*-grid is chosen proportionate to their unit cell size. Density of states (DOS) calculations for uniformly doped BC_x sheets are performed with a denser 15 × 15 × 1 *k*-grid. Gaussian smearing with a smearing width of 0.1 eV has been used for electronic structure calculations. The dynamic stability of these sheets has been investigated by calculating the phonon spectrum using the Parlinski–Li–Kawazoe method as implemented in the PHONOPY[61,62] package. The potential energy surface for Li over the BC_x sheets has been scanned using single point calculations and the energy barriers for Li-ion diffusion are evaluated using the Nudged Elastic Band (NEB) method.[63] While performing lithiation in these BC_x sheets, all the possible inequivalent positions for Li adsorption for a particular Li concentration have been considered and formation energies are calculated in order to obtain the convex hull as a function of Li concentration. In order to understand the thermal stability of the BC_2 sheets, *ab initio* molecular dynamics (AIMD) simulations were performed using a Nosé thermostat with a time step of 2 fs and a 3 × 3 × 1 *k*-grid.

3 Results and discussion

We first construct mono-layers of uniformly boron doped graphene by replacing a few C atoms with B in a super-cell of graphene. The resulting sheets have stoichiometry of BC_x, where x = 7, 5, 3, 2 and 1, as shown in Fig. 1(a–e) from left to right. The optimized lattice parameters of these BC_x sheets are reported in Table 1. We compare the lattice parameters of uniformly doped BC_x sheets with respect to graphene as a

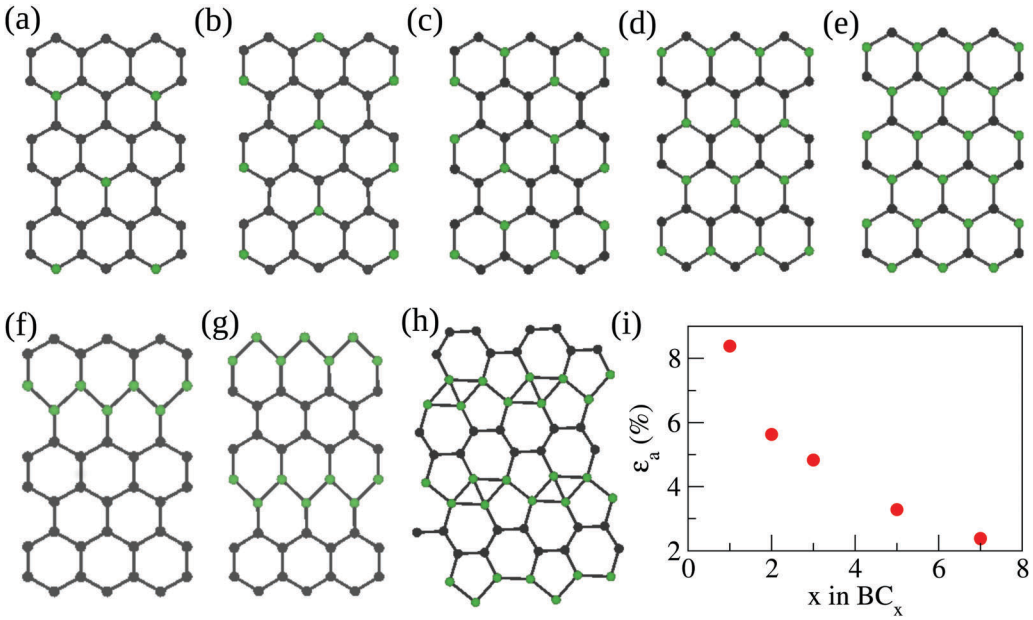

Fig. 1 Relaxed geometries of monolayer BC_x sheets with increasing concentrations of boron doping. Upper panels (uniformly B doped structures): (a) BC_7, (b) BC_5, (c) BC_3, (d) BC_2 and (e) BC. Lower panels (non-uniformly B doped structures): (f) BC_5-II, (g) BC_2-II and (h) BC-II. The green circles indicate boron atoms and black circles represent C. (i) Change in the lattice parameter ($\varepsilon_a = \frac{a - a_{gr}}{a} \times 100$, where a_{gr} is the lattice parameter of graphene having the same unit cell size as that of the BC_x sheet) for uniformly doped BC_x sheets as a function of B concentration.

Table 1 Lattice parameters (a and b) and Li adsorption energies (E_{ad}) for one Li in BC_x (x = 7, 3, 5, 2 and 1) sheets as a function of increasing boron concentration. Uniformly and non-uniformly doped structures have hexagonal and rectangular unit cells, respectively

Structure	a (Å)	E_{ad} (eV)	Structure	a and b (Å)	E_{ad} (eV)
BC_7	5.04	−1.90			
BC_5	7.63	−1.85	BC_5-II	13.5, 2.42	−0.72
BC_3	5.17	−0.77			
BC_2	7.82	−1.35	BC_2-II	2.42, 7.96	−1.62
BC_1	5.37	−4.99	BC-II	5.46, 4.33	−1.08

function of B concentration in Fig. 1(i). As expected, the lattice parameter of these sheets with respect to graphene increases with increasing B concentration due to longer C–B bonds (bond length ~1.52 Å). These B doped graphene sheets, except BC_2, have either been experimentally synthesized[39–41] or predicted theoretically.[36,64–66] The bonding structure of B_xC_{1-x} thin films, determined by XANES, shows that there is a structural transition at $x \sim 0.5$ from B_{12}-icosahedral units for the B-rich samples to hexagonal-like structures for the C-rich samples.[67] The phonon spectra of BC_3[41] show it to be dynamically stable and it also has been experimentally synthesized on the NbB_2 (0001) surface.[39] BC_5 has been synthesized using the chemical vapour deposition method and a possible structure of a monolayered BC_5 sheet has been suggested.[40] A uniformly doped BC_7 sheet has been theoretically predicted.[65] We have calculated the phonon spectra for the BC_2 sheet as shown in Fig. S1(a) (ESI†). The absence of negative frequency confirms the dynamic stability of the sheet. Furthermore, the formation energies of these sheets have been calculated as shown in Fig. S1(b) (ESI†). The corresponding details of the calculations are provided in the ESI.† Although the formation processes of these sheets are endothermic, the energy values are very small and do not change significantly for BC_7, BC_5, BC_3, and BC_2. Given the fact that BC_3 and BC_5 are already being synthesized, there is a great chance that BC_2 can also be synthesized. In order to assess the stability of these sheets during the charging/discharging process due to lattice expansion, we calculate the in-plane stiffness C_s[68] and compare it with graphene.[69] The calculated C_s values of uniformly doped BC, BC_2, BC_3, BC_5 and BC_7 are 275.12 N m^{-1}, 300.25 N m^{-1}, 317.99 N m^{-1}, 351.99 N m^{-1} and 357.82 N m^{-1}, respectively. C_s decreases as a function of B concentration, however, the values do not differ much from that of graphene (340 N m^{-1}). Therefore, like graphene, these sheets are expected to maintain their structural integrity during the charging/discharging process.

Furthermore, we have considered the energetically most preferable configurations for BC_5, BC_2 and BC (named as BC_5-II, BC_2-II and BC-II) having non-uniform arrangement of boron, obtained using the particle swarm optimization (PSO) technique.[38] It has been found that the formation of 1D boron zigzag chains is preferred in BC_5 and BC_2 as shown in Fig. 1(f and g). The hexagons having three B atoms in these two sheets are elongated due to B–B bonds (bond length ~1.70 Å). However, the minimum energy configuration of BC contains alternate strips of boron chains and armchair carbon chains as shown in Fig. 1(h). These three non-uniformly doped BC_x sheets are reported to be dynamically stable based on their phonon spectrum.[38] The relative energies per atom for these most preferable structures are 0.03, 0.01, and 0.3 eV lower compared to the uniformly doped cases for BC_5, BC_2 and BC, respectively. The low energy differences for BC_5 and BC_2 indicate that uniformly

doped structures can also exist as metastable structures during experimental growth of these sheets. All these B doped monolayers are planar and maintain the honeycomb lattice structure similar to graphene except, BC-II.

One of the requirements for a good anode material is that Li should bind to these sheets with an optimum adsorption energy. The adsorption energy should be strong enough to bind Li during charging. However, it should not be very high to hinder Li diffusion to the cathode during discharging. The adsorption energies (E_{ad}) have been calculated using the following equation:

$$E_{ad}(n) = E_{BC_x+n\mathrm{Li}} - E_{BC_x} - nE_{\mathrm{Li}}, \quad (1)$$

where $E_{BC_x+n\mathrm{Li}}$, E_{BC_x}, and E_{Li} are the energies corresponding to sheets with n adsorbed Li and without any Li, and the cohesive energy of bulk (bcc) Li, respectively. Table 1 lists the energies for adsorbing one Li on the monolayer BC_x sheets. In the case of uniformly doped BC_x sheets, the adsorption energy increases with decrease in B concentration for x = 2, 5 and 7 except in BC_3. The structures of both uniformly and non-uniformly doped BC_x sheets with one adsorbed Li are shown in Fig. S2 in the ESI.† When the B : C ratio is equal, the adsorption energy becomes very high leading to a high degree of buckling in BC. Since boron doping makes graphene electron deficient, it facilitates Li adsorption through a complete charge transfer from Li to the doped graphene. BC with the highest B concentration among all BC_x sheets is the most charge deficient and hence, adsorbs Li very strongly. Moreover, the structure of BC, having larger equivalent hexagons unlike other uniformly doped BC_x sheets, causes the strong Li adsorption. In BC_2, upon one Li adsorption, the structure buckles slightly near Li. The BC_x sheets with x = 3, 5 and 7 do not show any buckling and remain planar even after adsorbing one Li as shown in Fig. S2 (ESI†). For non-uniformly doped BC_x sheets, while BC_2-II and BC-II structures remain planar after adsorbing one Li, BC_5-II shows slight buckling.

In carbon based anode materials, the optimal range of adsorption energy[11] lies within 0–2 eV, beyond which Li diffusion during discharging will be hindered.[70,71] Although Li is adsorbed in uniformly doped BC, high binding energy will hinder the kinetics of Li ions. Additionally, upon adsorption of Li, the BC sheet ripples indicating instability. Therefore, we discard the BC phase from the list of potential candidates for anode materials. On the other hand, in the case of non-uniformly B doped systems, the adsorption energies for BC_5-II, BC_2-II and BC-II fall within the optimal range.

It has been shown that Li prefers to diffuse across the basal plane of doped graphene sheets instead of penetrating the hexagons of the sheets.[11] In order to determine the in-plane kinetics of Li, the potential energy surface (PES) of Li[12] in these sheets has been scanned as shown in Fig. S3 (ESI†). It captures an energy barrier profile that one Li will encounter while moving over the plane of BC_x. In Fig. 2, Li diffusion paths in uniformly doped BC_2, BC_5 and BC_7 sheets as well as in non-uniformly doped BC_5-II, BC_2-II and BC-II have been shown by dotted lines and the corresponding energy barriers have been plotted. Energy minima have been shown for each sheet with the red solid circle.

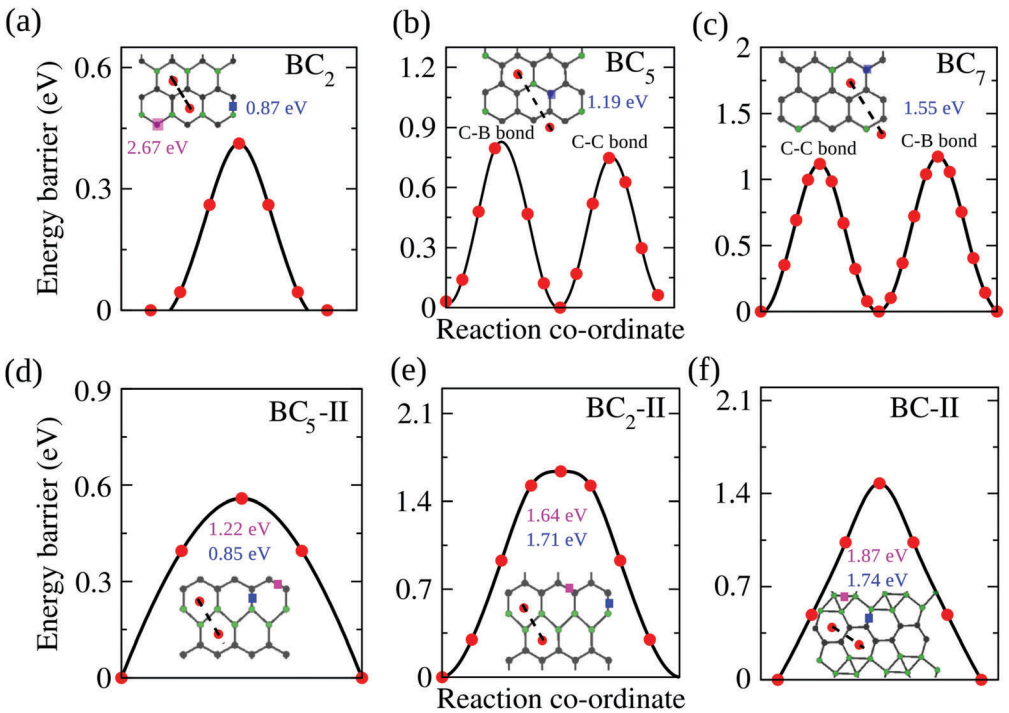

Fig. 2 Energy barriers for Li diffusion along the minimum energy path over (a) BC_2, (b) BC_5, (c) BC_7, (d) BC_5-II, (e) BC_2-II and (f) BC-II, respectively. The number of intermediate images is not the same for different sheets as the minimum energy path goes over different local arrangements of atoms for each sheet. The values in blue and magenta colors denote the energy barrier for Li diffusion at the sites marked by the same coloured box.

The energy barriers at different places such as over the C–C and C–B bond, have been shown in blue and magenta colors and the corresponding sites are marked with the same colored squares in Fig. 2. In the case of uniformly doped BC_2, the energy minimum shown by a red circle is at the centre of hexagons containing two B atoms placed vertically at the two corners, as shown in Fig. 2. The maximum energy barrier of 2.67 eV is obtained when the Li is on top of the C atom bonded to one C and two B atoms. The minimum energy path in BC_2 is along the direction over the C–C bonds having the lowest energy barrier of 0.41 eV as shown in Fig. 2(a), avoiding the B–C bonds with a high energy barrier of 0.87 eV. In the case of BC_3, Liu *et al.* reported that, at high Li concentration, Li diffuses with a barrier of 0.40 eV (similar to BC_2) by a vacancy hopping mechanism.[16] Next, in BC_5, all the hexagons are equivalent having one C atom replaced by a B atom. Li prefers to adsorb in the center of any hexagon and Li diffuses along any direction over both C–C and C–B bonds with energy barriers of 0.75 eV and 0.8 eV, respectively, as shown in Fig. 2(b). The energy barrier of 1.19 eV is observed when the Li is on top of the B atom. A BC_7 sheet consists of two types of hexagons having (i) all carbon atoms and (ii) one C atom replaced by a B atom. The energy minima for Li adsorption lie at the center of the second type of hexagon. Li faces energy barriers of 1.12 eV and 1.17 eV while crossing C–C and C–B bonds, respectively, in the BC_7 sheet as shown in Fig. 2(c). A high energy barrier of 1.55 eV has been found when Li is on the top of the C atom. We observe that the presence of B atoms in BC_x sheets facilitates Li adsorption causing energy minima closer to B atoms and hence, more energy is required for Li to diffuse over the B doped region resulting in a high energy barrier over B–C bonds compared to C–C bonds. In BC_2, due to higher concentration of B, elongated B–C bonds are more and there is a narrow channel of the C–C bond (bond length reduces to 1.34 Å) over which Li diffuses with the lowest energy barrier of 0.41 eV.

In the cases of non-uniformly doped BC_x structures, Li prefers to adsorb at the centre of the hexagons having three boron atoms in BC_5-II and BC_2-II. The minimum energy paths for these two cases lie along a zigzag path with an energy barrier of 0.56 eV and 1.47 eV, respectively, over the B–B bond as shown in Fig. 2(d) and (e), avoiding the high energy barrier of 0.85 eV and 1.71 eV, respectively, over the B–C bond. In these two cases, Li prefers to adsorb on both sides of a 1D B zigzag chain and makes the one-dimensional region close to B atoms energetically very low for Li diffusion unlike uniformly doped cases. The energy barrier over the C–C bond is very high, 1.22 eV and 1.64 eV for BC_5-II and BC_2-II respectively. In BC-II, Li adsorbs at the centre of the hexagon with two boron doped atoms due to larger hole compared to pentagons and boron triangular rings. The diffusion of Li will occur across these hexagons having an energy barrier of 1.47 eV over the C–C bond as shown in Fig. 2(f). The energy barrier over the B–B bond is very high, 1.87 eV due to the closely located B atoms in the boron triangular ring. Owing to the high diffusion barrier, BC_2-II and BC-II cannot be considered as good anode materials. Based on the energy barriers, Li diffuses faster across uniformly doped BC_x sheets with increasing B concentration having the lowest energy barrier in the case of BC_3 and BC_2. The lowering of the energy barriers indicates better Li kinetics and therefore, uniformly doped BC_x sheets except BC and only BC_5-II among non-uniformly doped BC_x sheets can be used as promising anode materials for Li ion batteries. Our assumptions regarding the relative kinetics of Li in these BC_x sheets are based on the fact that the prefactor in the Arrhenius equation remains constant. According to this equation, the mean jump frequency of Li at a temperature T is given by

$$\omega = \nu e^{(-E_b/k_B T)}. \quad (2)$$

The prefactor ν depends on the lattice vibrations at the initial and saddle-point states. The value of this prefactor is typically approximated by a constant value of the order of 10^{13} s^{-1}.[72,73] The height of diffusion barrier E_b, which is in the exponential part of eqn (2), plays the dominant role in determining Li kinetics. However, we cannot completely neglect the effect of the prefactor and it may affect Li kinetics. The complete estimation of these prefactors for all these sheets are computationally expensive and currently beyond the scope of this study.

Next, with a good understanding of kinetics, the gravimetric capacity of these sheets has been studied by calculating the adsorption energy as a function of Li concentration using eqn (1). Li atoms have been adsorbed one by one in these sheets. The trend of Li adsorption provides insight into Li–Li interactions along with the storage capacity and operating voltage of the anode/cathode materials. A negative slope in the incremental formation energy indicates favourable adsorption of more Li, while a positive slope indicates clustering of Li and formation of dendrites. We have checked the convex hull by considering different inequivalent positions for Li adsorptions on one-side and both-sides of the sheets and the formation energies are marked by open blue circles and orange diamonds, respectively, as shown in the upper panels in Fig. 3. The most preferable structures for different Li concentrations (marked by solid symbols) have been connected with solid lines. The point at which the slope reverses determines the concentration of Li in the BC_x sheet. The concentrations of Li in BC_2, BC_5, BC_5-II and BC_7 turn out to be $Li_{2.17}BC_2$, $Li_{1.33}BC_5$, Li_1BC_5-II and Li_1BC_7, respectively, for one-sided lithiation. These Li saturated phases are shown in Fig. S4 in the ESI† and it is found that for the uniformly doped BC_2 case, a maximum amount of Li can be stored due to an extra layer of Li adsorption. After occupying all the center positions of the hexagons for the first layer of Li adsorption at 1.70 Å above the sheet, the second layer of Li adsorption happens at 4.16 Å above the sheet and Li adsorbs at the positions in between the first layers of Li and B atoms of the sheet. This multilayer adsorption of Li/Na atoms will show enhanced specific capacity similar to earlier reported cases for other sheets such as borophene[53] and Mo_2C monolayers.[74]

After determining the saturated phase of Li in the BC_x sheet, the capacity C (mA h g^{-1}) is determined using the following formula:[75]

$$C = \frac{1}{A_c}\left[\left(\frac{p}{100}\right)\nu F 10^3\right], \quad (3)$$

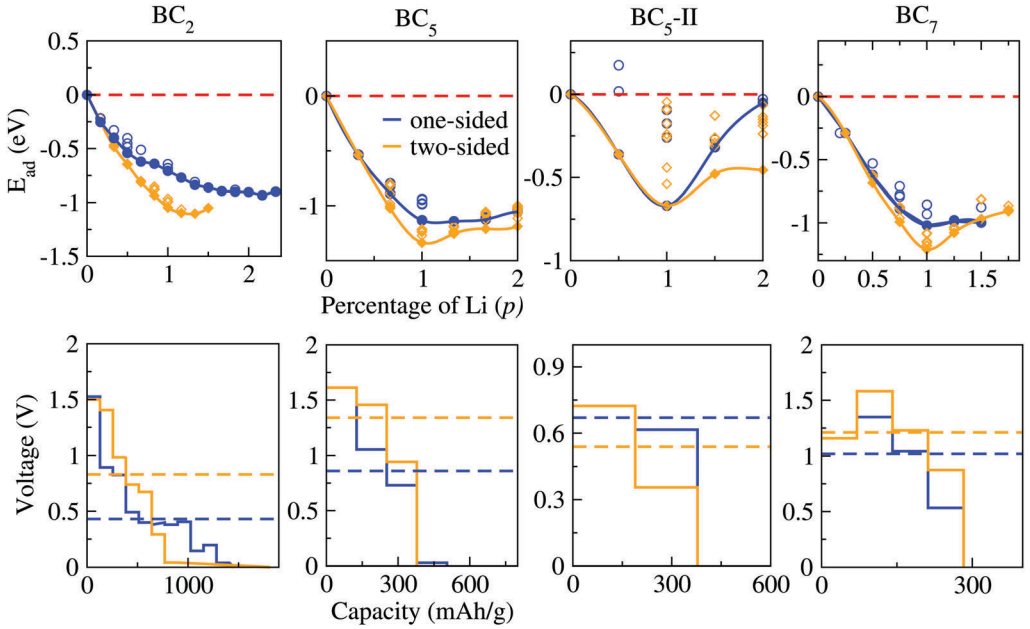

Fig. 3 Upper panels: Adsorption energy (E_{ad}) per formula unit as a function of percentage of Li (p) adsorbed per one unit of BC_x and lower panels: voltage *vs.* capacity (mA h g^{-1}) corresponding to BC_2, BC_5, BC_5-II and BC_7 (from left to right), respectively. In the upper panel, the different points in open blue circles (one-sided) and orange diamonds (two-sided) for a given Li concentration denote the formation energies for different structures having Li adsorbed at different positions of the sheet. The most preferable structures for different Li concentrations (marked by solid symbols) are connected by the solid lines. The dotted lines in the lower panels denote the average voltage.

where A_c is the atomic mass of BC_x, F is the Faraday constant (26.801 A h g^{-1}), p is percentage of Li adsorbed per one unit of BC_x and ν is the valency of Li (1). The concentrations of $Li_{2.17}BC_2$, $Li_{1.33}BC_5$, Li_1BC_5-II and Li_1BC_7 correspond to a capacity of 1667, 504, 378 and 283 mA h g^{-1}, respectively. A similar trend is observed in the two-sided capacity with concentrations of $Li_{1.33}BC_2$, Li_1BC_5, Li_1BC_5-II and Li_1BC_7 (structures are shown in Fig. S4, ESI†) corresponding to a capacity of 1026, 378, 378 and 283 mA h g^{-1}. Thus an increase in the B concentration has a pronounced effect on the capacity of the boron doped graphene and we find that uniformly doped BC_5 gives higher capacity than non-uniformly doped BC_5-II for one-sided lithiation. In Fig. 4, the capacity for both one and two-sided lithiation in all BC_x phases has been plotted. BC_2 has the highest ever capacity for B doped graphene sheets (higher than the earlier reported capacity of BC_3 marked in Fig. 4 for comparison[16]) making it an excellent candidate for high capacity anode materials in Li ion batteries. We have also checked the thermal stability of the BC_2 sheet at different temperatures (300, 500 and 750 K) using AIMD simulations. The structure remains intact even at a high temperature of 750 K as shown in Fig. S5(a and b) in the ESI.† Furthermore, the stability of the Li saturated phase of BC_2 has also been assessed using AIMD simulations at 300 K. The structure remains stable as shown in Fig. S5(c) (ESI†).

Another quantity of interest is the open circuit voltage, which has to be low for anode materials in order to get high voltage difference between the cathode and anode of Li ion batteries. The operating voltage of the battery is calculated by taking Li metal as the reference electrode.[76,77] The OCV ($\bar{V}$)

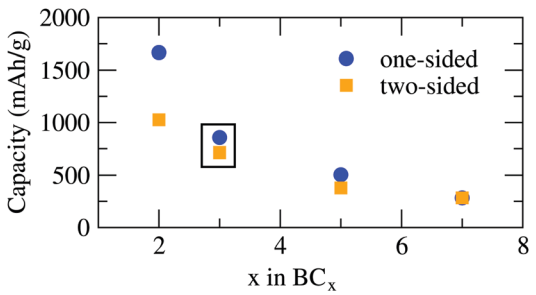

Fig. 4 Capacity as a function of the number of C atoms (x) per unit of uniformly doped BC_x sheets. The boxed data is adopted from a previous study by Liu *et al.*[16] The blue circles represent the capacity for one-sided lithiation of the BC_x monolayer and orange squares represent corresponding two-sided data.

can be estimated from the difference in Gibbs free energy, ΔG, using the following equation:

$$\bar{V} = -\frac{\Delta G}{\Delta n z F} \quad (4)$$

where F is the Faraday constant, Δn denotes the difference in the number of Li ion at two different compositions during charging/discharging and z = 1 is the electronic charge of the Li ions. Due to negligible contribution from the volume and entropy terms, ΔG can be approximated to ΔE_{ad}. Thus the final form for $\bar{V}$ during lithiation/delithiation between n_1 and n_2 Li, in terms of volts, is as follows:

$$\bar{V} = -\frac{E_{ad}(n_2) - E_{ad}(n_1)}{F \times (n_2 - n_1)}, \quad (5)$$

where $E_{ad}(n)$ is the formation energy for n Li. A negative value of OCV indicates no more adsorption of Li on the BC_x sheet. In the lower panels of Fig. 3, OCV has been plotted with respect to capacity for each BC_x sheet. To obtain the maximum voltage in Li ion batteries in the presence of a cathode, the OCV of the anode with respect to Li metal has to be low. During lithiation, the OCV profile should remain flat to achieve good performance.[78] The average voltages obtained for BC_2, BC_5, BC_5-II and BC_7 are 0.43 V, 0.86 V, 0.67 V and 1.02 V, respectively, for one-sided lithiation and 0.83 V, 1.34 V, 0.54 V and 1.21 V, respectively, for two-sided lithiation marked by dotted lines in Fig. 3. It is clear from Fig. 3 that the OCV profile remains low in BC_2 and BC_5-II, being minimum in BC_2 for one-sided lithiation. Hence, the uniformly doped BC_2 sheet shows the best performance with a low diffusion barrier, highest capacity as well as a low and flat voltage profile.

After finding the capacity and average voltage of these sheets, the energy density can be calculated by multiplying the voltage of a battery and specific capacity. Energy density defines the amount of energy stored in the battery per unit mass or volume and therefore, is a very important quantity to assess the overall performance of a battery. Considering the cathode half-cell voltage with respect to Li metal as 3.7 V corresponding to commercially used $LiCoO_2$,[79] we calculated the working voltage, *i.e.*, the voltage difference between the cathode and anode, in Li ion batteries. In the case of one-sided lithiation, the energy density peaks at a remarkably high value of 5451 W h kg^{-1} for BC_2, almost double the previously reported value for BC_3.[16] For the cases of BC_5, BC_5-II and BC_7, the values are 1431, 1145 and 758 W h kg^{-1}, respectively. Two-sided lithiation gives a slightly lower value of energy density: 2945, 892, 1194 and 705 W h kg^{-1} for BC_2, BC_5, BC_5-II and BC_7, respectively.

In order to understand why BC_2 shows such an extremely high capacity among all other BC_x phases, density of states (DOS) has been calculated for uniformly doped BC_x sheets as shown in Fig. 5(a) and (b) for the sheets without Li and after adsorbing one Li, respectively. Partial DOS for B-2p and Li-2s have been plotted in green and red solid colors, respectively. B doping in graphene provides empty states above the Fermi level, where Li can easily donate its electron.[10,80] We find that the number of available states in the conduction band increases with increasing B concentration. However, the states just above the Fermi level within a few eV, will be filled first during lithiation. The average number of available empty states above the Fermi level up to 2 eV (marked by brown solid bands) in uniformly doped BC_2 as shown in Fig. 5(a) is maximum compared to other BC_x sheets. The quantitative plot in Fig. 5(c) indeed confirms the maximum availability of empty states for the uniformly doped BC_2 sheet, which indicates that BC_2 can adsorb more Li causing multilayer adsorption. This clearly explains the superiority of uniformly doped BC_2 having the highest capacity among all B doped graphene derivatives. In Fig. 5(b), a Li-2s peak observed above the Fermi level denotes that Li is ionized and the position of this peak from the Fermi level denotes the amount of charge transfer from Li to the sheet. In uniformly doped BC, the Li-2s peak lies far from the Fermi level compared to other cases implying the highest charge transfer from the Li to BC sheet leading to high adsorption energy. The position of the Li-2s peak is the closest to the Fermi level for BC_3 followed by BC_2 denoting less amount of charge transfer for BC_3, which explains its lowest adsorption energy.

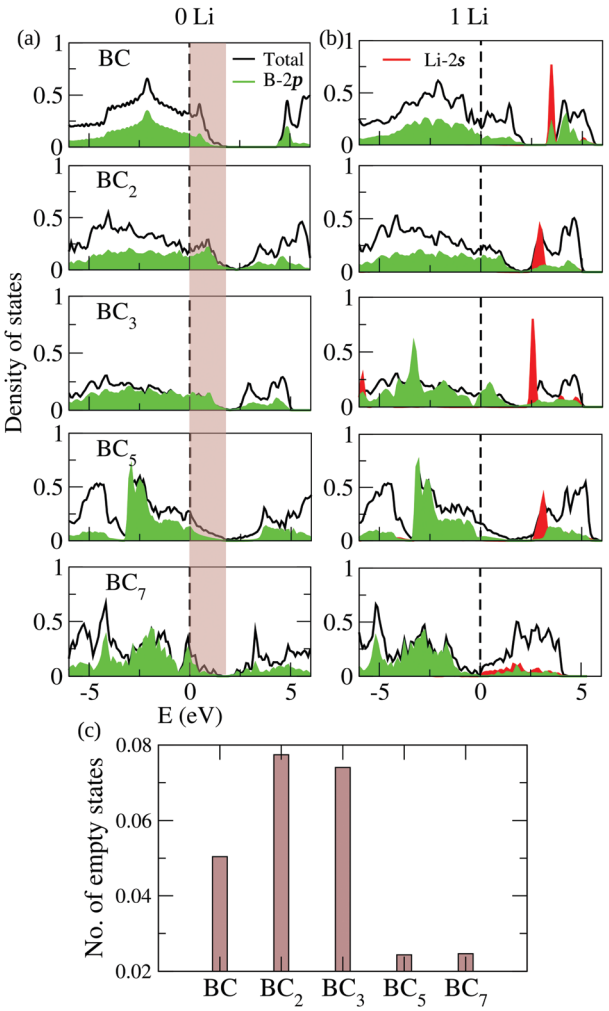

Fig. 5 Total and partial density of states for uniformly doped BC_x sheets, where x = 1, 2, 3, 5 and 7 from top to bottom, respectively, for (a) without Li and (b) with one Li adsorbed. (c) Average number of empty B-2p states above the Fermi level up to 2 eV for different BC_x sheets.

In order to explain the lithiation process in BC_x sheets and to investigate the saturation limit of Li, we have checked the change in partial density of states (PDOS) as a function of Li concentration. In BC_x sheets, Li has been absorbed one by one. For each adsorbed Li, we have calculated the adsorption energies for all the symmetrically inequivalent sites. The minimum energy configuration is chosen for adsorption of the next Li atom as mentioned above. PDOS has been calculated for these minimum energy configurations. Plots of B-2p and Li-2s states with increasing number of Li for uniformly doped BC_2 are shown in Fig. 6(a) and (b), respectively. With the increasing concentration of Li in the sheet, the empty states of B-2p above the Fermi level fill up with electrons donated by Li. The number of available empty states reduces and goes to a minimum at the

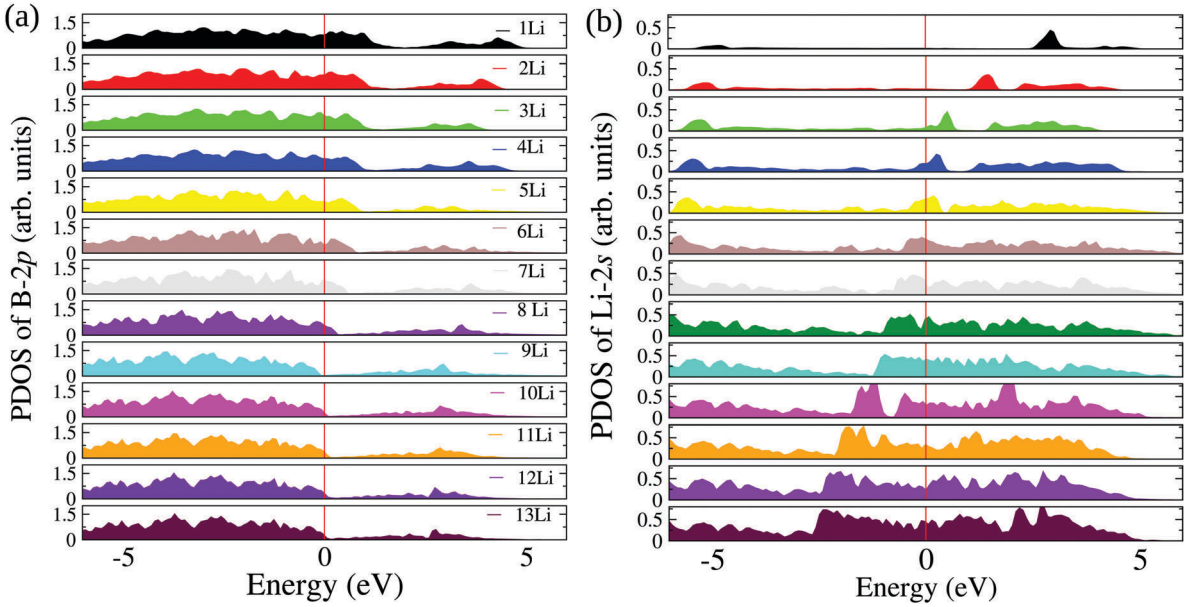

Fig. 6 Change in partial density of states for (a) B-2p and (b) Li-2s in BC_2 during lithiation. As the number of adsorbed Li increases, the empty B-2p states above the Fermi level fill up and shift below.

saturation value after which the sheet cannot adsorb anymore Li. The peak in Li-2s states above the Fermi level (as shown in Fig. 6(b)) shifts towards the left with an increasing amount of Li indicating the reduction in the strength of interaction between Li and the sheet. During lithiation, Li–Li interaction gradually increases and eventually the charge transfer from Li to the sheet decreases. In other sheets, the same trend has been observed as shown in Fig. S6 (ESI†) for uniformly doped BC_3, BC_5 and BC_7 sheets. The range over which the Li-2s peak in uniformly doped BC_2 shifts towards the Fermi level and crosses it is the largest among all the other sheets denoting maximum Li adsorption.

4 Conclusions

In summary, we have studied the feasibility of uniformly as well as non-uniformly B doped graphene as an anode material by varying the B concentration. Increasing the B concentration up to $x = 2$ in the BC_x phase leads to enhancement in capacity and low diffusion barrier. We found that uniformly doped BC_2 shows a remarkably high capacity of 1667 (1026) mA h g^{-1} within the optimal Li adsorption energy limit for one-sided (two-sided) lithiation. This is the highest ever reported for boron doped graphene sheets and this extremely high capacity can be attributed to the maximum number of available empty states in BC_2 just above the Fermi level and the multilayer Li adsorption mechanism for one-sided lithiation. Besides showing better Li kinetics, it also gives a low and flat voltage profile making it an excellent candidate for Li ion batteries. However, in the uniformly doped BC sheet ($x = 1$), Li binds strongly due to a higher concentration of B that impedes the delithiation process and in non-uniformly doped BC and BC_2 sheets the energy barriers for Li diffusion are very high, rendering them ineffective as an anode material. Our study provides a collective understanding of inter-related chemical and electrical performance of uniform and non-uniform B doped graphene based anode materials for Li ion batteries, which can be generalised to develop high performance and more viable high-capacity, low-cost anodes. With the recent rapid development in controlled synthesis of B doped graphitic structures, BC_2 has a great chance of being experimentally realized in the very near future.

Conflicts of interest

There are no conflicts to declare.

Acknowledgements

The authors are thankful for the financial support from Korea Institute of Science and Technology (Grant No. 2E25372). Kwang-Ryeol Lee and Sang Soo Han were supported by the Industrial Strategic Technology Development Program (Grant No. 10041589) funded by the Ministry of Knowledge Economy (MKE, Korea). We also thank the Materials Research Centre and Supercomputer Education and Research Centre, Indian Institute of Science for the computing facilities.

References

1 J.-M. Tarascon and M. Armand, *Nature*, 2001, **414**, 359–367.
2 Y. Nishi, *J. Power Sources*, 2001, **100**, 101–106.
3 B. Kang and G. Ceder, *Nature*, 2009, **458**, 190–193.
4 M. Armand, S. Grugeon, H. Vezin, S. Laruelle, P. Ribière, P. Poizot and J.-M. Tarascon, *Nat. Mater.*, 2009, **8**, 120–125.
5 M. Morcrette, P. Rozier, L. Dupont, E. Mugnier, L. Sannier, J. Galy and J.-M. Tarascon, *Nat. Mater.*, 2003, **2**, 755–761.
6 K. Zaghib, A. Mauger, H. Groult, J. B. Goodenough and C. M. Julien, *Materials*, 2013, **6**, 1028–1049.

7 K. Kang, Y. S. Meng, J. Bréger, C. P. Grey and G. Ceder, *Science*, 2006, **311**, 977–980.
8 C. K. Chan, H. Peng, G. Liu, K. McIlwrath, X. F. Zhang, R. A. Huggins and Y. Cui, *Nat. Nanotechnol.*, 2008, **3**, 31–35.
9 A. S. Aricó, P. Bruce, B. Scrosati, J.-M. Tarascon and W. van Schalkwijk, *Nat. Mater.*, 2005, **4**, 366–377.
10 D. Das, S. Kim, K.-R. Lee and A. K. Singh, *Phys. Chem. Chem. Phys.*, 2013, **15**, 15128–15134.
11 R. P. Hardikar, D. Das, S. S. Han, K.-R. Lee and A. K. Singh, *Phys. Chem. Chem. Phys.*, 2014, **16**, 16502–16508.
12 D. Das, S. S. Han, K.-R. Lee and A. K. Singh, *Phys. Chem. Chem. Phys.*, 2014, **16**, 21688–21693.
13 P. Lian, X. Zhu, S. Liang, Z. Li, W. Yang and H. Wang, *Electrochim. Acta*, 2010, **55**, 3909–3914.
14 E. Yoo, J. Kim, E. Hosono, H.-s. Zhou, T. Kudo and I. Honma, *Nano Lett.*, 2008, **8**, 2277–2282.
15 E. Lee and K. A. Persson, *Nano Lett.*, 2012, **12**, 4624–4628.
16 Y. Liu, V. I. Artyukhov, M. Liu, A. R. Harutyunyan and B. I. Yakobson, *J. Phys. Chem. Lett.*, 2013, **4**, 1737–1742.
17 X. Zhao, C. M. Hayner, M. C. Kung and H. H. Kung, *ACS Nano*, 2011, **5**, 8739–8749.
18 A. L. M. Reddy, A. Srivastava, S. R. Gowda, H. Gullapalli, M. Dubey and P. M. Ajayan, *ACS Nano*, 2010, **4**, 6337–6342.
19 X. Fan, W. Zheng and J.-L. Kuo, *ACS Appl. Mater. Interfaces*, 2012, **4**, 2432–2438.
20 L. S. Panchakarla, K. S. Subrahmanyam, S. K. Saha, A. Govindaraj, H. R. Krishnamurthy, U. V. Waghmare and C. N. R. Rao, *Adv. Mater.*, 2009, **21**, 4726–4730.
21 S. Han, D. Wu, S. Li, F. Zhang and X. Feng, *Small*, 2013, **9**, 1173–1187.
22 P. Ayala, J. Reppert, M. Grobosch, M. Knupfer, T. Pichler and A. M. Rao, *Appl. Phys. Lett.*, 2010, **96**, 183110.
23 S. Wu, W. Ren, L. Xu, F. Li and H.-M. Cheng, *ACS Nano*, 2011, **5**, 5463–5471.
24 X. Wang, Z. Zeng, H. Ahn and G. Wang, *Appl. Phys. Lett.*, 2009, **95**, 183103.
25 Y.-C. Lin, C.-Y. Lin and P.-W. Chiu, *Appl. Phys. Lett.*, 2010, **96**, 133110.
26 H. Wang, C. Zhang, Z. Liu, L. Wang, P. Han, H. Xu, K. Zhang, S. Dong, J. Yao and G. Cui, *J. Mater. Chem.*, 2011, **21**, 5430–5434.
27 R. Lu, D. Rao, Z. Meng, X. Zhang, G. Xu, Y. Liu, E. Kan, C. Xiao and K. Deng, *Phys. Chem. Chem. Phys.*, 2013, **15**, 16120–16126.
28 H.-Q. Xiang, S.-B. Fang and Y.-Y. Jiang, *Solid State Ionics*, 2002, **148**, 35–43.
29 Z.-S. Wu, W. Ren, L. Xu, F. Li and H.-M. Cheng, *ACS Nano*, 2011, **5**, 5463–5471.
30 V. L. Solozhenko, O. O. Kurakevych, D. Andrault, Y. Le Godec and M. Mezouar, *Phys. Rev. Lett.*, 2009, **102**, 015506.
31 P. Lazar and R. Podloucky, *Appl. Phys. Lett.*, 2009, **94**, 177–182.
32 Q. Li, H. Wang, Y. Tian, Y. Xia, T. Cui, J. He, Y. Ma and G. Zou, *J. Appl. Phys.*, 2010, **108**, 023507.
33 L. Xu, Z. Zhao, L.-M. Wang, B. Xu, J. He, Z. Liu and Y. Tian, *J. Phys. Chem. C*, 2010, **114**, 22688–22690.
34 L. Xu, Z. Zhao, Q. Wang, L.-M. Wang, B. Xu, J. He and Y. Tian, *J. Appl. Phys.*, 2011, **110**, 013501.
35 J. Dai, Z. Li, J. Yang and J. Hou, *Nanoscale*, 2012, **4**, 3032–3035.
36 F. J. Ribeiro and M. L. Cohen, *Phys. Rev. B: Condens. Matter Mater. Phys.*, 2004, **69**, 212507.
37 D. Y. Wang, Q. Yan, B. Wang, Y. X. Wang, J. Yang and G. Yang, *J. Chem. Phys.*, 2014, **140**, 224704.
38 X. Luo, J. Yang, H. Liu, X. Wu, Y. Wang, Y. Ma, S.-H. Wei, X. Gong and H. Xiang, *J. Am. Chem. Soc.*, 2011, **133**, 16285–16290.
39 C. Oshima, *J. Phys.: Condens. Matter*, 2012, **24**, 314206.
40 B. M. Way, J. R. Dahn, T. Tiedje, K. Myrtle and M. Kasrai, *Phys. Rev. B: Condens. Matter Mater. Phys.*, 1992, **46**, 1697–1702.
41 H. Yanagisawa, T. Tanaka, Y. Ishida, M. Matsue, E. Rokuta, S. Otani and C. Oshima, *Phys. Rev. Lett.*, 2004, **93**, 177003.
42 C. Oshima, *J. Phys.: Condens. Matter*, 2012, **24**, 314206.
43 P. V. Zinin, L. C. Ming, H. A. Ishii, R. Jia, T. Acosta and E. Hellebrand, *J. Appl. Phys.*, 2012, **111**, 114905.
44 C. Ling and F. Mizuno, *Phys. Chem. Chem. Phys.*, 2014, **16**, 10419–10424.
45 S. Agnoli and M. Favaro, *J. Mater. Chem. A*, 2016, **4**, 5002–5025.
46 E. Rodríguez, I. Cameán, R. García and A. B. García, *Electrochim. Acta*, 2011, **56**, 5090–5094.
47 U. Tanaka, T. Sogabe, H. Sakagoshi, M. Ito and T. Tojo, *Carbon*, 2001, **39**, 931–936.
48 E. J. Mele and J. J. Ritsko, *Phys. Rev. B: Condens. Matter Mater. Phys.*, 1981, **24**, 1000–1005.
49 L. Zhou, Z. F. Hou, B. Gao and T. Frauenheim, *J. Mater. Chem. A*, 2016, **4**, 13407–13413.
50 M. Lalitha, S. S. Mahadevan and S. Lakshmipathi, *J. Mater. Sci.*, 2016, 1–17.
51 H. Jiang, Z. Lu, M. Wu, F. Ciucci and T. Zhao, *Nano Energy*, 2016, **23**, 97–104.
52 Y. Zhang, Z.-F. Wu, P.-F. Gao, S.-L. Zhang and Y.-H. Wen, *ACS Appl. Mater. Interfaces*, 2016, **8**, 22175–22181.
53 X. Zhang, J. Hu, Y. Cheng, H. Y. Yang, Y. Yao and S. A. Yang, *Nanoscale*, 2016, **8**, 15340–15347.
54 B. Mortazavi, A. Dianat, O. Rahaman, G. Cuniberti and T. Rabczuk, *J. Power Sources*, 2016, **329**, 456–461.
55 B. Mortazavi, O. Rahaman, S. Ahzi and T. Rabczuk, *Appl. Mater. Today*, 2017, **8**, 60–67.
56 G. Kresse and J. Hafner, *Phys. Rev. B: Condens. Matter Mater. Phys.*, 1993, **47**, 558–561.
57 G. Kresse and D. Joubert, *Phys. Rev. B: Condens. Matter Mater. Phys.*, 1999, **59**, 1758–1775.
58 P. E. Blóchl, *Phys. Rev. B: Condens. Matter Mater. Phys.*, 1994, **50**, 17953–17979.
59 J. P. Perdew, K. Burke and M. Ernzerhof, *Phys. Rev. Lett.*, 1996, **77**, 3865–3868.
60 G. Kresse and J. Furthmuller, *Comput. Mater. Sci.*, 1996, **6**, 15–50.
61 A. Togo, F. Oba and I. Tanaka, *Phys. Rev. B: Condens. Matter Mater. Phys.*, 2008, **78**, 134106.

62 A. Togo and I. Tanaka, *Scr. Mater.*, 2015, **108**, 1–5.
63 G. Henkelman, B. P. Uberuaga and H. Jónsson, *J. Chem. Phys.*, 2000, **113**, 9901.
64 Q. Hu, Q. Wu, Y. Ma, L. Zhang, Z. Liu, J. He, H. Sun, H.-T. Wang and Y. Tian, *Phys. Rev. B: Condens. Matter Mater. Phys.*, 2006, **73**, 214116.
65 J. E. Lowther, *J. Phys.: Condens. Matter*, 2005, **17**, 3221.
66 M. M. Li, X. Fan and W. T. Zheng, *J. Phys.: Condens. Matter*, 2013, **25**, 425502.
67 I. Caretti, R. Gago, J. M. Albella and I. Jiménez, *Phys. Rev. B: Condens. Matter Mater. Phys.*, 2008, **77**, 174109.
68 B. R. Sharma, A. Manjanath and A. K. Singh, *Sci. Rep.*, 2014, **4**, 7164.
69 C. Lee, X. Wei, J. W. Kysar and J. Hone, *Science*, 2008, **321**, 385–388.
70 B. J. Landi, M. J. Ganter, C. D. Cress, R. A. DiLeo and R. P. Raffaelle, *Energy Environ. Sci.*, 2009, **2**, 638–654.
71 H. J. Hwang, J. Koo, M. Park, N. Park, Y. Kwon and H. Lee, *J. Phys. Chem. C*, 2013, **117**, 6919–6923.
72 A. Van der Ven, G. Ceder, M. Asta and P. D. Tepesch, *Phys. Rev. B: Condens. Matter Mater. Phys.*, 2001, **64**, 184307.
73 Z. Wang, A. P. Ratvik, T. Grande and S. M. Selbach, *RSC Adv.*, 2015, **5**, 15985–15992.
74 D. Cakir, C. Sevik, O. Gulseren and F. M. Peeters, *J. Mater. Chem. A*, 2016, **4**, 6029–6035.
75 D. Datta, J. Li and V. B. Shenoy, *ACS Appl. Mater. Interfaces*, 2014, **6**, 1788–1795.
76 M. K. Aydinol, A. F. Kohan, G. Ceder, K. Cho and J. Joannopoulos, *Phys. Rev. B: Condens. Matter Mater. Phys.*, 1997, **56**, 1354–1365.
77 M. Aydinol, A. Kohan and G. Ceder, *J. Power Sources*, 1997, **68**, 664–668.
78 J. B. Goodenough and Y. Kim, *Chem. Mater.*, 2010, **22**, 587–603.
79 G. Ceder, G. Hautier, A. Jain and S. Ong, *MRS Bull.*, 2011, **36**, 185–191.
80 D. H. Wu, Y. F. Li and Z. Zhou, *Theor. Chem. Acc.*, 2011, **130**, 209–213.